Activation of Peroxymonosulfate by $Fe^0@Fe_3O_4$ Core-Shell Nanowires for Sulfate Radical Generation: Electron Transfer and Transformation Products

Yong Feng[1,2], Jie Zhong[1,2], Liyuan Zhang[3], Yiang Fan[3], Zequn Yang[3], Kaimin Shih[3] *, Hailong Li[4], Deli Wu[5], Bo Yan[1,2] *

[1]SCNU Environmental Research Institute, Guangdong Provincial Key Laboratory of Chemical Pollution and Environmental Safety & MOE Key Laboratory of Theoretical Chemistry of Environment, South China Normal University, Guangzhou 510006, China

[2]School of Environment, South China Normal University, University Town, Guangzhou 510006, China

[3]Department of Civil Engineering, The University of Hong Kong, Pokfulam, Hong Kong, China

[4]School of Energy Science and Engineering, Central South University, Changsha 410083, China

[5]State Key Laboratory of Pollution Control and Resources Reuse, School of Environmental Science & Engineering, Tongji University, Shanghai 200092, China

Manuscript submitted to Separation and Purification Technology

Contacts:

Dr. Yong Feng (fengy@scnu.edu.cn)

Prof. Kaimin Shih (kshih@hku.hk)

*To whom correspondence should be addressed:

Professor Kaimin Shih

Phone: +852-2859-1973

Fax: +852-2559-5337

E-mail: kshih@hku.hk

ABSTRACT

Nanoscale zero-valent iron (nZVI) is highly promising for oxidative removal of micropollutants by initiating advanced oxidation processes, but its vulnerability to deactivation due to the surface oxidation is challenging. In this study, we propose $Fe^0@Fe_3O_4$ core-shell nanowires (CSNWs) as a novel activator to generate radicals for atrazine, a representative micropollutant, degradation via the activation of peroxymonosulfate (PMS). $Fe^0@Fe_3O_4$ CSNWs with a shell thickness of around 5 nm were synthesized using a facile chemical reduction approach and were comprehensively characterized using a series of surface sensitive techniques. The results showed that the $Fe^0@Fe_3O_4$ CSNW had great reactivity for atrazine degradation via the activation of PMS; near complete degradation of atrazine was achieved after reaction for only 2 min. Under identical conditions, the pseudo-first order rate constant with $Fe^0@Fe_3O_4$ was more than 36 times greater than that with nano Fe_3O_4. The surface activation of PMS contributed only a small proportion to the overall degradation. Instead, the iron released from $Fe^0@Fe_3O_4$ CSNWs primarily activated PMS to generate $SO_4^{\cdot-}$ that degraded atrazine. The $Fe^0@Fe_3O_4$ CSNWs were stable and no deactivation was observed after exposing $Fe^0@Fe_3O_4$ CSNWs to air for 3 months. The results from this study demonstrate a stable nZVI for oxidative removal of organic contaminants.

Keywords: Zero-valent iron; $Fe^0@Fe_3O_4$**;** core-shell nanowires; atrazine; peroxymonosulfate

1. Introduction

The widely occurrence of trace levels of microorganic contaminants in various environmental matrices requires the development of highly efficient remediation technologies [1, 2]. Sulfate radical ($SO_4^{\cdot-}$)-mediated treatments, recently emerged as a novel advanced oxidation process (AOP), have shown great promise in the degradation of various kinds of organic contaminants, such as antibiotics [3, 4] and endocrine disrupting chemicals [5, 6]. The generation of $SO_4^{\cdot-}$ depends on the activation of either peroxymonosulfate (PMS) or peroxydisulfate (PDS), and many activation technologies that rely on UV irradiation, heating, base, or transition metals have been proposed [7-9]. Of these activation technologies reported, the activation of PMS (PDS) by transition metals through an one-electron transfer mechanism (Eq. 1) [10-13] is very promising for practical environmental remediation applications, because such techniques do not require external energy and many of the transition metals are ubiquitous in soil and aquifers.

$$M^n + HSO_5^- \rightarrow M^{n+1} + SO_4^{\cdot-} + OH^- \quad (1)$$

Iron is an environmentally friendly and low-cost material. However, dissolved iron (e.g., Fe^{2+}, Fe^{3+}) [14] and iron oxides (e.g., Fe_2O_3 and Fe_3O_4) [15, 16] are relatively low efficient for $SO_4^{\cdot-}$-mediated AOPs due to the thermodynamically unfavorable reduction of Fe^{3+} by persulfates and the strong scavenging effect of Fe^{2+} toward $SO_4^{\cdot-}$ (4.6×10^9 M^{-1} s^{-1}, Eq. 2) [17-19]. To accelerate the regeneration of Fe^{2+}, many strategies, such as UV irradiation and addition of reducing agents [14, 20], have been reported. To mitigate the scavenging effect of Fe^{2+}, we have previously used structural ferrous iron-containing minerals, such as pyrite [21] and siderite [22], as sources of Fe^{2+}. However, the release of sulfate ions and bicarbonate ions may be a concern when high dosages of pyrite and siderite are used; bicarbonate ions are strong radical scavengers ($k_{HCO_3^-, SO_4^{\cdot-}} = (9.1 \pm 0.4) \times 10^6\ M^{-1}\ s^{-1}$) [23] and the resulting carbonate radical ($CO_3^{\cdot-}$; E^0 = 1.57 V) [24] is less oxidizing than $SO_4^{\cdot-}$ (E^0 = 2.5-3.1 V) [25].

$$Fe^{2+} + SO_4^{\cdot-} \rightarrow Fe^{3+} + SO_4^{2-} \quad (2)$$

Nanoscale zero-valent iron (nZVI) has been used as an activator in AOPs, particularly hydroxyl radical (·OH)-mediated processes [26, 27]. For the generation of $SO_4^{\cdot-}$ via persulfate activation, nZVI has also been studied [28, 29]. Although both nZVI-PDS and nZVI-PMS combinations can degrade a serious of organic contaminants, the scavenging effect of excess nZVI has been reported [30, 31]. In addition, the high surface energy of nZVI rends it easily aggregate and passivate in AOPs [32-34], in which dissolved oxygen is ubiquitously present. To solve these problems, we here propose to use Fe^0@Fe_3O_4 core-shell nanowires (CSNWs) to activate PMS. A Fe^0@Fe_3O_4 CSNW consists of a Fe^0 core and a surrounding thin shell of Fe_3O_4. Fe^0@Fe_3O_4 CSNWs provide an efficient interface for electron transport. The Fe_3O_4 shell can be considered as an n-type semiconductor, which mediates the electrons transfer from the Fe^0 core to the surface adsorbed contaminants [35, 36]. Therefore, the potential synergy between Fe^0 and Fe_3O_4 may aid the circulation of iron at different valent states and thus improve the activation of PMS.

In this study, Fe^0@Fe_3O_4 CSNWs were synthesized using a facile reduction approach and were used, for the first time, to activate PMS for the degradation of target contaminant atrazine, which is a widely used herbicide and has been frequently detected in various environmental matrices [37]. The nanowires prepared were fully characterized using various surface-sensitive techniques and their reactivity was tested under varied experimental conditions. To explore the activation mechanism, classical scavenging experiments and kinetic studies were carried out. Finally, the transformation product of Fe^0@Fe_3O_4 CSNWs was studied, and the electron transfer associated with the activation process was proposed.

2. Experimental section

2.1 Chemicals

OXONE, monopersulfate compound ($KHSO_5 \cdot 0.5KHSO_4 \cdot 0.5K_2SO_4$), ferrous sulfate heptahydrate (≥99.0%), sodium borohydride, sodium thiosulfate, nitrobenzene, and Pluronic F-127 were obtained from Sigma-Aldrich (St. Louis, MO, USA). Atrazine (97%) was supplied by TCI Ltd. (Shanghai, China). *tert*-Butanol (99.5%) was purchased from Aladdin Corp. (Shanghai, China). High-performance liquid chromatography (HPLC) grade methanol and sulfuric acid (2 M) were supplied by Fisher Scientific (Pittsburgh, PA, USA). Ultrapure water (18.0 MΩ · cm) for preparing experimental solutions was prepared using a Millipore water purification system.

2.2 Synthesis and characterization of $Fe^0@Fe_3O_4$ CSNWs

$Fe^0@Fe_3O_4$ CSNWs were synthesized using a facile reduction method. In a typical procedure, 6 g of ferrous sulfate heptahydrate, 4.1 g of sodium borohydride, and 1 g of Pluronic F-127 were dissolved in 50 mL, 10 mL, and 40 mL of ultrapure water, respectively. The resulting ferrous sulfate solution was then mixed with the F-127 solution, followed by the dropwise addition of the sodium borohydride solution to produce black powders. The black powders obtained were washed with pure ethanol and deoxygenated water to remove impurities. The resulting products were put in a freeze-drying device and dried for 12 h. The mechanism underling the formation of Fe_3O_4 layer on nano Fe^0 cores is described by Eqs.3 and 4 [38]. Nano Fe_3O_4 was synthesized using a solvothermal approach [39].

$$2Fe^0 + O_2 \rightarrow 2FeO \quad (3)$$

$$6FeO + O_2 \rightarrow 2Fe_3O_4 \quad (4)$$

The purity and crystallinity of the synthesized sample were characterized using a D8 Advance X-ray diffractometer (Bruker, Karlsruhe, Germany) with a Cu X-ray tube at 40 mA and 40 kV.

The valent state of iron on the material surface was characterized using an ESCALAB 250XI X-ray photoelectron spectrometer (Thermo, Waltham, MA, USA) with Al−Kα radiation. The morphology was examined using a Hitachi S-4800 scanning electron microscope and a FEI Tecnai G2 20 S-TWIN transmission electron microscope. The measurement of Brunauer−Emmett−Teller specific surface area was carried out via N_2 adsorption at 77 K using an ASAP 2460 surface area analyzer (Micromeritics, Norcross, GA, USA). The Fourier-transform infrared (FT-IR) spectra were recorded on a Spectrum 100 FT-IR spectrometer (PerkinElmer, Waltham, MA, USA). The Zeta potential was measured using a Malvern Zeta potential analyzer (Malvern, UK), and the point of zero charge (pH_{pzc}) was estimated to be around 6.8.

2.3 Degradation experiments

Unless otherwise stated, all degradation reactions were conducted at room temperature (25 ± 1 ºC) in 200 mL glass reactors. In a typical test, 100 mL of atrazine solution (500 μg/L) was added to the glass reactor, followed by the addition of PMS solution. The original pH value of the atrazine solution with PMS (1 mM) was around 3.0 and was further adjusted when necessary using a diluted NaOH or H_2SO_4 solution. $Fe^0@Fe_3O_4$ CSNWs were then added to the solution to initiate activation and degradation reactions. Samples were withdrawn with syringes, filtered with PTFE membrane filters (0.22 μm), and transferred to autosampler vials (2 mL) for HPLC analysis. To prevent the atrazine from further degradation, excess sodium thiosulfate (10 μL, 0.5 M) was spiked to the vials. After the degradation reaction, the solid activators were recollected by vacuum filtration and dried in a freeze-drying device for further use. The degradation of atrazine by PMS alone is described in Note S1.

150 2.4 Chemical analysis

151 Atrazine was measured using an Agilent 1260 Infinity II HPLC system equipped with a diode
152 array detector (DAD) and an autosampler. The separation was carried out on a ZORBAX
153 Eclipse XDB-C18 column (4.6 × 150 mm, 5 μm). A mobile phase consisted of HPLC-grade
154 methanol and ultrapure water (60:40) was used for the elution. The flow rate and column
155 temperature were fixed at 1 mL/min and 30 ºC, respectively. The DAD wavelength was set at
156 222 nm. The retention time of atrazine was around 2.4 min. The solution pH was measured
157 using an Orion 2-Star benchtop pH meter. PMS was quantified using an iodometric method
158 [40], which is based on the quantification of I_3^-.

159

160 **3. Results and discussion**

161 3.1 Material characterization

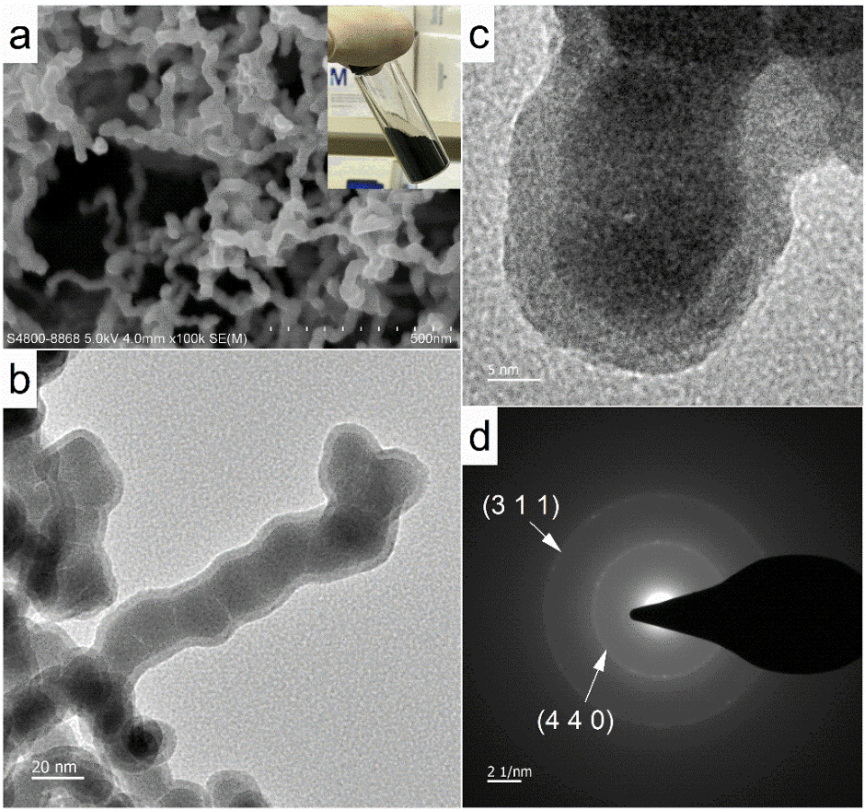

162

163 Figure 1. (a) Scanning electron microscopy, (b) transmission electron microscopy, (c) high-
164 resolution transmission electron microscopy, and (d) selected area electron diffraction images
165 of $Fe^0@Fe_3O_4$ CSNWs. The inset in (a) shows the image of the synthesized $Fe^0@Fe_3O_4$
166 CSNWs.

The scanning electron microscopy image shows that the synthesized sample existed in nanowire structures with a length of 200 to 300 nm (Fig. 1a). The nanowires consisted of core-shell structures (Fig. 1b) with a shell thickness of around 5 nm (Fig. 1c). The composition of the shell layer was investigated using selected area electron diffraction and was found to be Fe_3O_4 (Fig. 1d). The transmission electron microscopy image of nano Fe_3O_4 is shown in Fig. S1, which reveals that the size of the nano Fe_3O_4 was generally in the range of 10 to 20 nm.

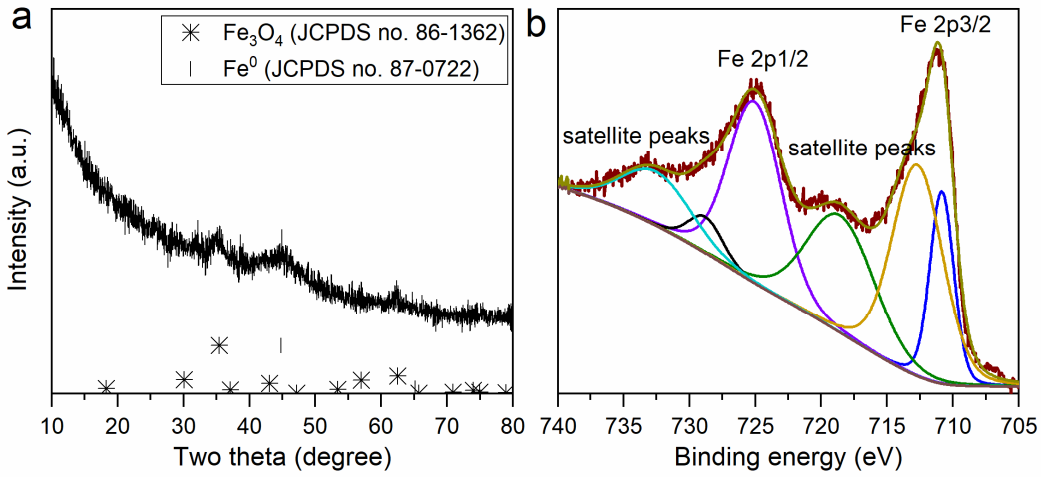

Figure 2. (a) X-ray diffraction pattern and (b) X-ray photoelectron spectroscopy spectrum of fresh $Fe^0@Fe_3O_4$ CSNWs.

The X-ray diffraction pattern of the synthesized $Fe^0@Fe_3O_4$ CSNW sample is shown in Fig. 2a. A weak and broad peak at around 45° is observed, which is a characteristic peak of metallic Fe^0 (JCPDS no. 87-722) [41]. The average size of the particle can be measured according to the Scherrer equation $D = k(\lambda/\beta \cos(\theta))$. Where λ is the X-ray wavelength equal to 0.154 nm, θ is the half diffraction angle, k is a constant equal to 0.89, and β is the full width at half maximum. When θ was at around 45°, β was measured to be 3.226. Therefore, the size of the metallic Fe^0 (nZVI) was calculated to be around 17 nm, which is very close to the value observed in Fig. 1b. The X-ray diffraction pattern of nano Fe_3O_4 is shown in Fig. S2. This pattern confirms that pure nano Fe_3O_4 (JCPDS no. 19-0629) was successfully synthesized. The specific surface areas of $Fe^0@Fe_3O_4$ CSNWs and nano Fe_3O_4 were measured to be 56.2 and

20.7 m^3/g, respectively. Other physical-chemical properties of the activators, such as pore size, are listed in Table S1.

The valent state of iron on $Fe^0@Fe_3O_4$ CSNWs was investigated using X-ray photoelectron spectroscopy. The highly resolution X-ray photoelectron spectrum of Fe is shown in Fig. 2b. Two bands with banding energies at around 711.2 and 725.1 eV were assigned to Fe $2p_{3/2}$ and Fe $2p_{1/2}$ [42], respectively. These bands are the characteristic peaks of Fe(II) from FeO and Fe(III) from Fe_3O_4 [16], which consistently suggests that the shell layer of the $Fe^0@Fe_3O_4$ CSNWs is Fe_3O_4.

3.2 Reactivity of $Fe^0@Fe_3O_4$ CSNWs

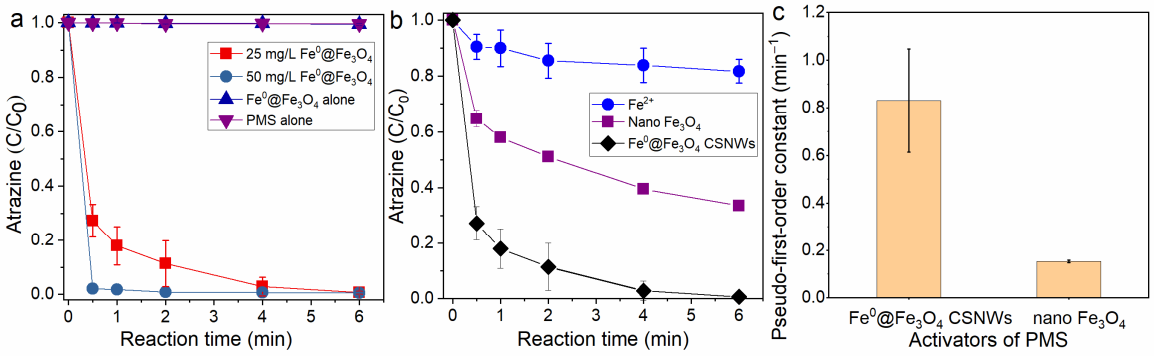

Figure 3. (a) Degradation of atrazine by $Fe^0@Fe_3O_4$ CSNWs-activated PMS, (b) comparison of different activators for atrazine degradation via the activation of PMS, and (c) pseudo-first-order rate constants with different activators. Conditions: [PMS] = 1 mM, [atrazine] = 500 µg/L, [$Fe^0@Fe_3O_4$ CSNWs] = [nano Fe_3O_4] = 25 mg/L, [Fe^{2+}] = 4 mg/L, and pH 3.0.

Only slight degradation of atrazine (<1%) occurred in the presence of PMS alone (pH 3–4; Fig. S3), which is consistent with the fact that PMS has quite limited oxidative capability under acidic conditions [43]. $Fe^0@Fe_3O_4$ CSNWs alone also had no obvious reactivity to remove atrazine (Fig. S4). When $Fe^0@Fe_3O_4$ CSNWs were co-present with PMS, rapid degradation of atrazine was observed; near complete degradation of atrazine was achieved after reaction for 2 min in the presence of 1 mM PMS and 50 mg/L $Fe^0@Fe_3O_4$ CSNWs (Fig. 3a). This rapid

degradation of atrazine suggests the efficient reactivity of $Fe^0@Fe_3O_4$ CSNWs toward PMS activation.

To reveal the potential synergy between the Fe^0 and Fe_3O_4 in $Fe^0@Fe_3O_4$ CSNWs, we studied the degradation of atrazine in the presence of the synthesized nano Fe_3O_4. Under identical conditions, $Fe^0@Fe_3O_4$ CSNWs had significant greater reactivity than nano Fe_3O_4 (Fig. 3b); approximately 100% degradation of atrazine was achieved with $Fe^0@Fe_3O_4$ CSNWs-PMS after reaction for 6 min, while only 66% of the degradation was achieved with nano Fe_3O_4-PMS. Kinetics investigations revealed that the removal of atrazine followed pseudo-first-order kinetics in the tested time range. The pseudo-first-order kinetic constant with $Fe^0@Fe_3O_4$ CSNWs-PMS was calculated to be around 0.216 min^{-1}, which was 36 times greater than that with nano Fe_3O_4-PMS (0.006 min^{-1}) (Fig. 3c). The reactivity of Fe^{2+} was also studied and compared. The selection of the concentration of Fe^{2+} (4 mg/L) was based on the leaching result of iron in the presence of PMS (Fig. 4c). The results show that an overall degradation rate of less than 20% was achieved by Fe^{2+}-PMS (Fig. 3b). This value was significantly lower than that obtained by $Fe^0@Fe_3O_4$ CSNWs-PMS (~100%), suggesting that $Fe^0@Fe_3O_4$ CSNWs had much higher reactivity than Fe^{2+}.

3.3 Effects of experimental parameters and active sites

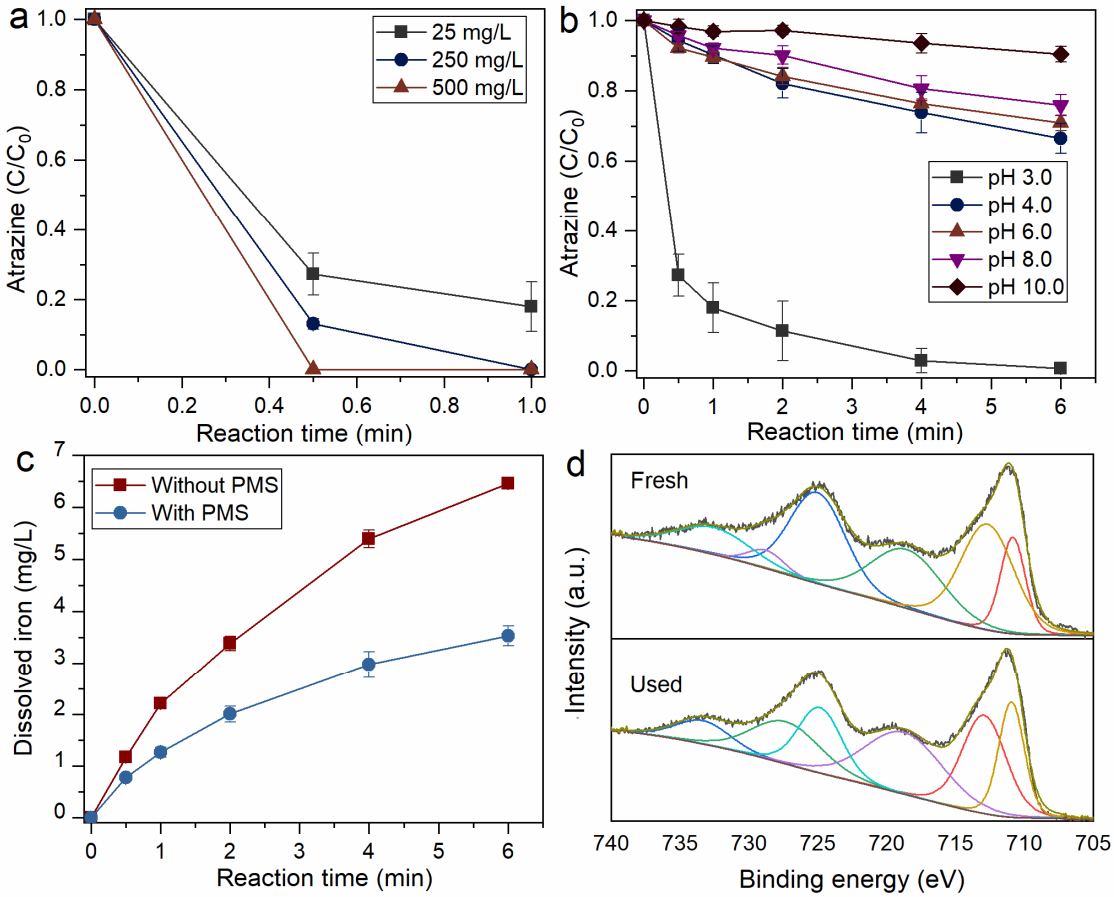

Figure 4. (a) Effects of $Fe^0@Fe_3O_4$ CSNWs and (b) pH value on the degradation of atrazine. (c) Iron leaching during the activation of PMS by $Fe^0@Fe_3O_4$ CSNWs. (d) High resolution X-ray photoelectron spectroscopy spectra of Fe 2p from fresh and used $Fe^0@Fe_3O_4$ CSNWs. Conditions: [PMS] = 1 mM, (b, c) [$Fe^0@Fe_3O_4$ CSNWs] = 25 mg/L, and pH 3.0.

The degradation of atrazine increased with the increase of $Fe^0@Fe_3O_4$ CSNW dosage from 25 to 500 mg/L, and no scavenging effect was observed (Fig. 4a). The effect of solution pH value on the activation of PMS by $Fe^0@Fe_3O_4$ CSNWs for atrazine degradation was studied. The degradation performance decreased significantly when the pH value rose from 3.0 to 4.0 (Fig. 4b). Only slight change in the degradation occurred when the pH value was in the range of 4.0 to 8.0, but an obvious decrease in the degradation was noticed when the pH value was further increased to 10.0. The significant decrease with the pH enhancement from 3.0 to 4.0 could be ascribed to the limited availability of dissolved iron. The total dissolved iron (TDI) under both

pH conditions was measured. Around 3.6 mg/L of TDI was detected when $Fe^0@Fe_3O_4$ CSNWs reacted with PMS for 6 min at pH 3.0 (Fig. 4c). However, the overall TDI was measured to be lower than 50 μg/L at pH 4.0. Such a low level of TDI had a negligible effect on the activation of PMS (Fig. S5). In the absence of PMS, the overall TDI was measured to be 6.5 mg/L, which was much greater than the value (3.6 mg/L) measured in the presence of PMS. The adverse effect of PMS on the leaching of iron was probably due to its adsorption onto the surface of $Fe^0@Fe_3O_4$ CSNWs, which hindered the interaction between H^+ and $Fe^0@Fe_3O_4$ CSNWs. This phenomenon was also observed in our previous study with siderite as the activator [22].

In the absence of $Fe^0@Fe_3O_4$ CSNWs, only 0.5% of the atrazine was degraded by PMS alone (Fig. S3). However, the degradation rate increased to around 34% when $Fe^0@Fe_3O_4$ CSNWs was present, which reveals that the surface activation of PMS by $Fe^0@Fe_3O_4$ CSNWs also occurred. Tan et al. [44] studied the activation of PMS by nanoscale Fe_3O_4 under different pH values, and they found that an increase in the acidity has an inhibitory effect. For such a reason, the contribution of the surface activation to the overall degradation performance at pH 3.0 should be much smaller than that at pH 4.0. Therefore, the heterogeneous activation of PMS by $Fe^0@Fe_3O_4$ CSNW surfaces occurred but should not be the key mechanism for the efficient degradation of atrazine. Instead, the dissolved iron was the major species for PMS activation. In addition, atrazine has a pK_a value of around 1.6 [45], which suggests that atrazine existed mainly as neutral molecules in the tested pH range. Thus, the low performance at pH 10 was not caused by static interaction. Instead, the dominance of SO_5^{2-} over HSO_5^- was probably the controlling factor. PMS has a second ionization constant of around 9.4 [46]; PMS exited mainly in form of SO_5^{2-} at pH 10.0. Compared with HSO_5^-, SO_5^{2-} is much more difficult to activate [15, 47]. As the pH_{pzc} of $Fe^0@Fe_3O_4$ CSNWs was around 6.8, their surfaces were negatively charged when the pH value of the reacting solution was in the range of 8.0 to 10.0. The

negatively charged surfaces were not electrostatically favorable to react with SO_5^{2-}.In addition, some PMS decomposed under alkaline conditions to generate nonradical species, which also probably contributed to the low performance [48, 49]. The high-resolution X-ray photoelectron spectroscopy spectra of Fe 2p from the fresh and used Fe^0@Fe_3O_4 CSNWs were recorded (Fig. 4d). By comparing these spectra, it can be seen that only slight oxidation of the surface iron occurred after the activation reaction.

3.4 Kinetics for atrazine degradation

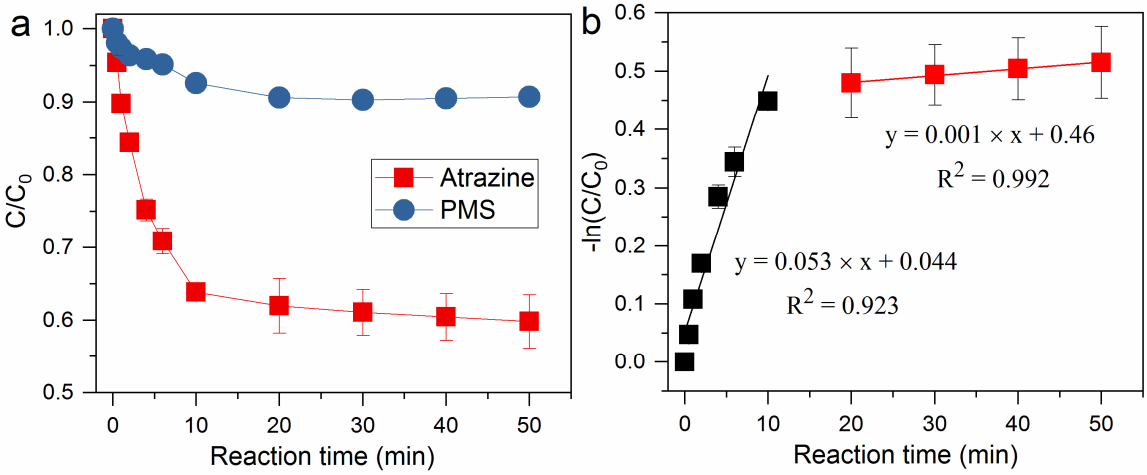

Figure 5. (a) Degradation of atrazine and decomposition of PMS. (b) Plot of -ln(C/C_0) versus reaction time (min). Conditions: [atrazine] = 5 mg/L, [Fe^0@Fe_3O_4 CSNWs] = 25 mg/L, [PMS] = 1 mM, and pH 3.0.

To investigate the kinetics, the degradation of atrazine with a relatively higher level of concentration (5 mg/L) was explored. Rapid degradation of atrazine was observed in the first 10 min and the rate slowed down with the continuation of the reaction (Fig. 5a). Meanwhile, relatively more rapid decrease in the concentration of PMS occurred in the first 10 min of reaction. To measure the efficiency of the oxidant, we calculated the stoichiometric efficiency (Eq. 5) [47]. Under the conditions of 5 mg/L atrazine and 1 mM PMS, the stoichiometric efficiency was calculated to be around 10.3%.

$$\text{Stoichiometric efficiency} = \frac{[\text{atrazine}]_0 - [\text{atrazine}]_{t=50\text{min}}}{[\text{PMS}]_0 - [\text{PMS}]_{t=50\text{min}}} \times 100\% \quad (5)$$

In $Fe^0@Fe_3O_4$ CSNWs-PMS oxidation, the fate of atrazine can be expressed by a pseudo-first-order law with regard to the concentration of atrazine (Eq. 6). An integration of Eq. 6 yields Eq. 7.

$$-\frac{d[\text{atrazine}]}{dt} = k_{app}[\text{atrazine}] \quad (6)$$

$$-\ln\left(\frac{[\text{atrazine}]}{[\text{atrazine}]_0}\right) = k_{app}t \quad (7)$$

As shown in Fig. 5b, there were two different reaction stages. Considering the transformation product of $Fe^0@Fe_3O_4$ CSNWs, it is easy to conclude that these two reaction stages were mainly mediated by the released Fe^{2+} and formed r-FeOOH. By plotting -ln[atrazine]/[atrazine]$_0$ versus reaction time (Eq. 7), the pseudo-first-order kinetic rate constants for atrazine degradation by Fe^{2+}-PMS and r-FeOOH-PMS were calculated to be 0.053 and 0.001 min^{-1}, respectively. The low reactivity of r-FeOOH toward PMS activation could be explained by the difficulty in the regeneration of Fe(II) from Fe(III) reduction.

3.5 Activation and degradation mechanisms

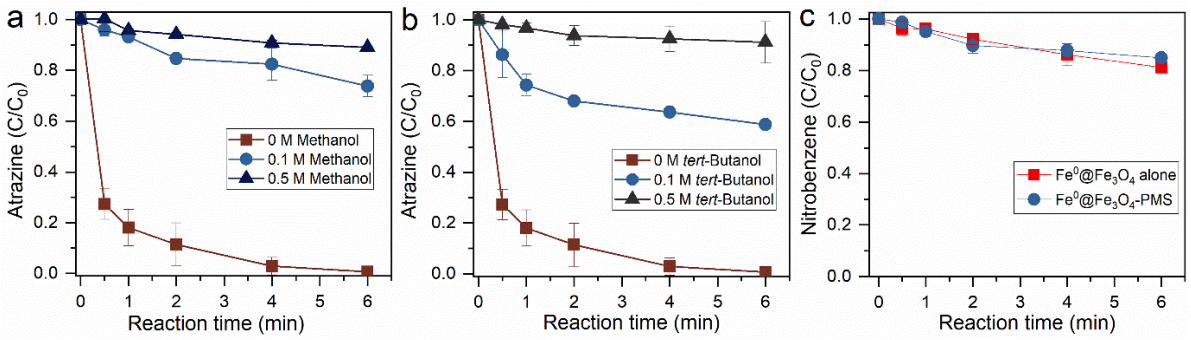

Figure 6. (a) Effects of methanol and (b) *tert*-butanol on the degradation of atrazine by $Fe^0@Fe_3O_4$ CSNWs-activated PMS. (c) Degradation of nitrobenzene by $Fe^0@Fe_3O_4$ CSNWs-activated PMS. Conditions: [atrazine] = 500 µg/L (2.3 µM), [$Fe^0@Fe_3O_4$ CSNWs] = 25 mg/L, [PMS] = 1 mM, and [nitrobenzene] = 2.3 µM.

To examine the degradation mechanism of atrazine, classical scavenging experiments were carried out to study the role of radicals. The scavenging experiments were based on the great difference in the reaction rate constants of alcohols (methanol and *tert*-butanol) with oxygen-bearing radicals. Methanol reacts rapidly with both ·OH (9.7×10^8 M^{-1} s^{-1}) [50] and $SO_4^{\cdot-}$ (1.0×10^7 M^{-1} s^{-1}) [51]. *tert*-Butanol is reactive for ·OH (3.3×10^9 M^{-1} s^{-1}), but highly inert for $SO_4^{\cdot-}$ ($4.1–9.0 \times 10^5$ M^{-1} s^{-1}). The results show that the degradation of atrazine was significantly inhibited in the presence of 0.1 M of methanol, and the inhibitory extent was increased with the further enhancement of methanol dose; the overall degradation rate was decreased from around 99% to 10% when 0.5 M methanol was present (Fig. 6a). Significant inhibitory effects were also observed when different levels of *tert*-butanol presented as a scavenger; the overall degradation rate was decreased from around 99% to 9% when 0.5 M of *tert*-butanol was present (Fig. 6b). The significant scavenging effects of both methanol and *tert*-butanol suggest the dominance of radicals in the degradation.

To further examine the radical species produced, the degradation of nitrobenzene by Fe^0@Fe_3O_4 CSNWs-PMS was investigated. Nitrobenzene reacts quite slowly with $SO_4^{\cdot-}$ ($<10^6$ M^{-1} s^{-1}), but interacts rapidly with ·OH (3.9×10^9 M^{-1} s^{-1}) [50]. Our previous work has shown the effectiveness of using nitrobenzene in the identification of $SO_4^{\cdot-}$ [52]. Less than 20% of the nitrobenzene was removed by Fe^0@Fe_3O_4 CSNWs alone and no obvious change in the removal performance was observed when PMS was further added (Fig. 6c). This observation suggests that the combination of Fe^0@Fe_3O_4 CSNWs with PMS had no obvious oxidizing capability toward nitrobenzene, and therefore $SO_4^{\cdot-}$ was the dominant active species.

$$Fe^0 + O_2 + 2H^+ \rightarrow Fe^{2+} + H_2O_2 \quad (8)$$

$$Fe^{2+} + H_2O_2 \rightarrow Fe^{3+} + \cdot OH + OH^- \quad (9)$$

$$\equiv Fe^{III}OH + Fe^{2+} + H_2O \rightarrow \equiv Fe^{III}OFe^{II}OH + 2H^+ \quad (10)$$

$$\equiv Fe^{III}OFe^{II}OH \rightarrow \equiv Fe^{II}OFe^{III}OH \quad (11)$$

$$\equiv Fe^{II}OFe^{III}OH + O_2 \rightarrow \equiv Fe^{III}OFe^{III}OH + \cdot O_2^- \quad (12)$$

$$Fe^0 + 2Fe^{3+} \rightarrow 3Fe^{2+} \quad (13)$$

$$Fe^{3+} + \cdot O_2^- \rightarrow Fe^{2+} + O_2 \quad (14)$$

Previous studies reported that $\cdot OH$ could be generated via the activation of dissolved molecular oxygen by nZVI (Eqs. 8 and 9) [53, 54]. However, the dominance of $SO_4^{\cdot -}$ in $Fe^0@Fe_3O_4$ CSNWs-PMS oxidation suggests that the contribution of this mechanism to the degradation was negligible. The significant greater reactivity of $Fe^0@Fe_3O_4$ CSNWs over Fe_3O_4 could be ascribed to the accelerated regeneration of both structural Fe(II) and dissolved Fe^{2+}. First, the $\equiv Fe^{III}OH$ on $Fe^0@Fe_3O_4$ CSNWs formed a complex ($\equiv Fe^{III}OFe^{II}OH$) with the released Fe^{2+} (Eq. 10). Second, electron transfer occurred in the complex and resulted in the formation of $\equiv Fe^{II}OFe^{III}OH$ (Eq. 11), which then activated dissolved molecular oxygen to produce superoxide radicals ($\cdot O_2^-$; Eq. 12). Finally, the produced $\cdot O_2^-$ along with the Fe^0 core reduced Fe^{3+} to Fe^{2+} (Eqs. 13 and 14) [41, 55]. In addition to the facilitate the regeneration of Fe^{2+}, the Fe_3O_4 shell well prevented the Fe^0 core from deactivation. To further reveal this protection, we exposed the $Fe^0@Fe_3O_4$ CSNWs in air for three months and then compared their reactivity for PMS activation with fresh $Fe^0@Fe_3O_4$ CSNWs. The results show that no obvious difference in the degradation of atrazine was observed with the two kinds of $Fe^0@Fe_3O_4$ CSNWs (Fig. S6).

The morphology of the $Fe^0@Fe_3O_4$ CSNWs after its extended reaction with PMS was investigated. The emission scanning microscopy image shows that needle-like products were formed during the transformation of $Fe^0@Fe_3O_4$ CSNWs (Fig. 7a). The X-ray diffraction characterization showed that sharp crystalline peaks were recorded and lepidocrocite (r-FeOOH; JCPDS no. 44-1415) was the major oxidation product (Fig. 7b). This finding was

further supported by the FT-IR studies (Fig. 7c) and selected area electron diffraction pattern (Fig. 7d). The generation of r-FeOOH as the major product of nZVI oxidation is consistent with previous reports [33, 56].

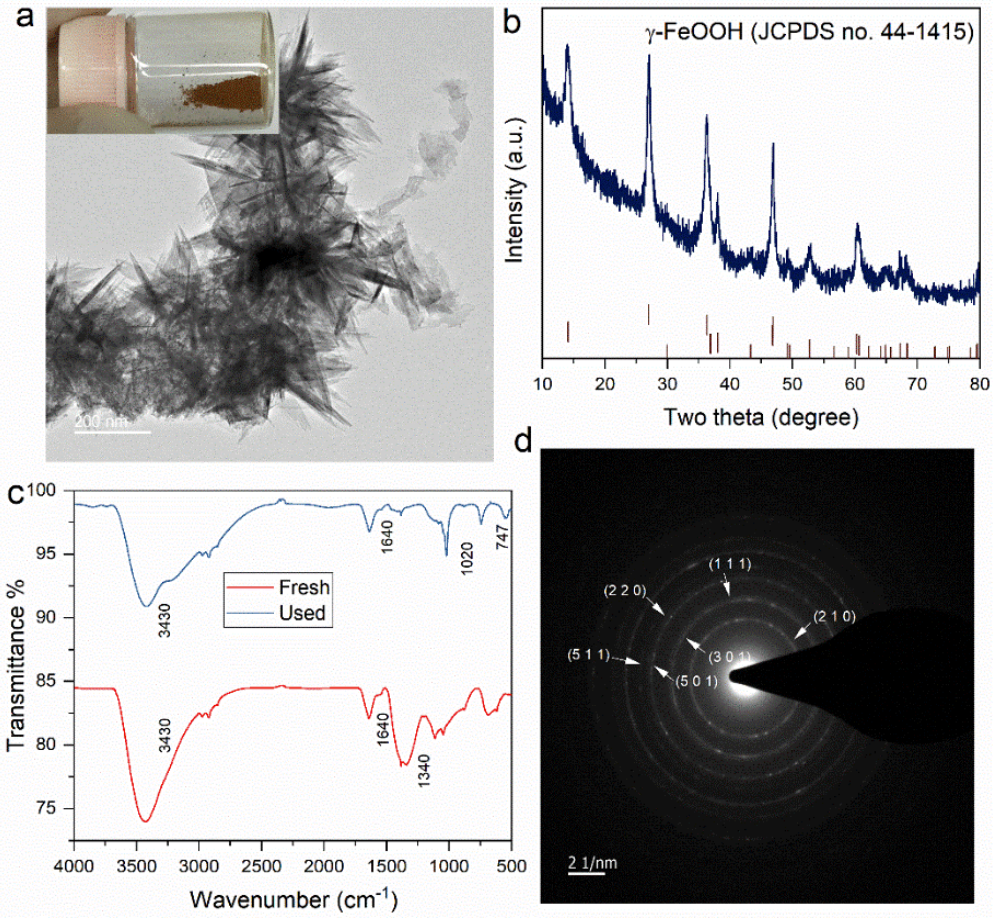

Figure 7. (a) Transmission electron microscopy image, (b) X-ray diffraction pattern, (c) FI-TR spectra, and (d) selected area electron diffraction pattern of the $Fe^0@Fe_3O_4$ CSNWs after an extended reaction with PMS. The inset in (a) shows the image of the used $Fe^0@Fe_3O_4$ CSNWs.

4 Conclusions

Although iron-based core-shell structures have previously been studied in ·OH-mediated AOPs, they are rarely investigated in $SO_4^{\cdot-}$ -mediated processes, particularly through the activation of PMS. In this study, $Fe^0@Fe_3O_4$ CSNWs were synthesized and demonstrated to be a highly efficient activator of PMS for atrazine removal from water solutions. Some conclusions can be drawn as follows:

(1) $Fe^0@Fe_3O_4$ CSNWs with a shell layer thickness of 5 nm was successfully synthesized using the facile reduction approach;

(2) $Fe^0@Fe_3O_4$ CSNWs had high reactivity for atrazine degradation via the activation of PMS; near 100% removal of atrazine was achieved after reaction for 2 min in the presence of 1 mM PMS and 50 mg/L $Fe^0@Fe_3O_4$ CSNWs;

(3) $Fe^0@Fe_3O_4$ CSNWs had significantly greater reactivity than nano Fe_3O_4. The rate constant with $Fe^0@Fe_3O_4$ CSNWs was calculated to be around 0.216 min^{-1}, which was 36 times that with nano Fe_3O_4 (0.006 min^{-1});

(4) The surface activation of PMS by $Fe^0@Fe_3O_4$ CSNWs occurred, but this mechanism contributed only a small proportion to the degradation of atrazine. Instead, the iron released from $Fe^0@Fe_3O_4$ CSNWs primarily activated PMS to generate $SO_4^{\cdot-}$ that degraded atrazine;

(5) Two reaction stages were observed in the activation of PMS by $Fe^0@Fe_3O_4$ CSNWs, which was found to be caused by the generation of r-FeOOH from $Fe^0@Fe_3O_4$ CSNW oxidation;

(6) The $Fe^0@Fe_3O_4$ CSNWs are highly stable in air, which suggests convenience during the transportation and storage in practical remediation applications.

(7) A low stoichiometric efficiency (10.3%) was recorded, which reveals that the majority of the PMS was invalidly consumed during the activation process.

Acknowledgements

This study was funded by the Research Grants Council of Hong Kong (Projects 106180082, C7044-14G, and T21-711/16R), the start-up fund from South China Normal University (8S0597), and the Guangdong Basic and Applied Basic Research Fund.

List of Contents in SI

References

[1] R.P. Schwarzenbach, B.I. Escher, K. Fenner, T.B. Hofstetter, C.A. Johnson, U. Von Gunten, B. Wehrli, The challenge of micropollutants in aquatic systems, Science, 313 (2006) 1072-1077.

[2] P.J. Alvarez, C.K. Chan, M. Elimelech, N.J. Halas, D. Villagrán, Emerging opportunities for nanotechnology to enhance water security, Nat. Nanotechnol., 13 (2018) 634.

[3] W. Tian, H. Zhang, X. Duan, H. Sun, M.O. Tade, H.M. Ang, S. Wang, Nitrogen- and sulfur-codoped hierarchically porous carbon for adsorptive and oxidative removal of pharmaceutical contaminants, ACS Appl. Mater. Interfaces, 8 (2016) 7184-7193.

[4] Y. Ji, Y. Fan, K. Liu, D. Kong, J. Lu, Thermo activated persulfate oxidation of antibiotic sulfamethoxazole and structurally related compounds, Water Res., 87 (2015) 1-9.

[5] X. Wang, Y. Qin, L. Zhu, H. Tang, Nitrogen-doped reduced graphene oxide as a bifunctional material for removing bisphenols: Synergistic effect between adsorption and catalysis, Environ. Sci. Technol., 49 (2015) 6855-6864.

[6] G.X. Huang, C.Y. Wang, C.W. Yang, P.C. Guo, H.Q. Yu, Degradation of bisphenol A by peroxymonosulfate catalytically activated with $Mn_{1.8}Fe_{1.2}O_4$ nanospheres: Synergism between Mn and Fe, Environ. Sci. Technol., 51 (2017) 12611-12618.

[7] B.T. Zhang, Y. Zhang, Y. Teng, M. Fan, Sulfate radical and its application in decontamination technologies, Crit. Rev. Environ. Sci. Technol., 45 (2015) 1756-1800.

[8] W.D. Oh, Z.L. Dong, T.T. Lim, Generation of sulfate radical through heterogeneous catalysis for organic contaminants removal: Current development, challenges and prospects, Appl. Catal., B, 194 (2016) 169-201.

[9] Y. Wang, D. Tian, W. Chu, M. Li, X. Lu, Nanoscaled magnetic $CuFe_2O_4$ as an activator of peroxymonosulfate for the degradation of antibiotics norfloxacin, Sep. Purif. Technol., 212 (2019) 536-544.

[10] G.P. Anipsitakis, D.D. Dionysiou, Radical generation by the interaction of transition metals with common oxidants, Environ. Sci. Technol., 38 (2004) 3705-3712.

[11] P. Hu, M. Long, Cobalt-catalyzed sulfate radical-based advanced oxidation: A review on heterogeneous catalysts and applications, Appl. Catal., B, 181 (2016) 103-117.

[12] C. Su, X. Duan, J. Miao, Y. Zhong, W. Zhou, S. Wang, Z. Shao, Mixed conducting perovskite materials as superior catalysts for fast aqueous-phase advanced oxidation: A mechanistic study, ACS Catalysis, 7 (2017) 388-397.

[13] G. Chen, X. Zhang, Y. Gao, G. Zhu, Q. Cheng, X. Cheng, Novel magnetic $MnO_2/MnFe_2O_4$ nanocomposite as a heterogeneous catalyst for activation of peroxymonosulfate (PMS) toward oxidation of organic pollutants, Sep. Purif. Technol., 213 (2019) 456-464.

[14] J. Zou, J. Ma, L. Chen, X. Li, Y. Guan, P. Xie, C. Pan, Rapid acceleration of ferrous iron/peroxymonosulfate oxidation of organic pollutants by promoting Fe(III)/Fe(II) cycle with hydroxylamine, Environ. Sci. Technol., 47 (2013) 11685-11691.

[15] T. Zhang, H. Zhu, J.P. Croué, Production of sulfate radical from peroxymonosulfate induced by a magnetically separable $CuFe_2O_4$ spinel in water: Efficiency, stability, and mechanism, Environ. Sci. Technol., 47 (2013) 2784-2791.

[16] S. Zhang, Q. Fan, H. Gao, Y. Huang, X. Liu, J. Li, X. Xu, X. Wang, Formation of $Fe_3O_4@MnO_2$ ball-in-ball hollow spheres as a high performance catalyst with enhanced catalytic performances, J. Mater. Chem. A., 4 (2016) 1414-1422.

[17] G.V. Buxton, T.N. Malone, G.A. Salmon, Reaction of SO_4^- with Fe^{2+}, Mn^{2+} and Cu^{2+} in aqueous solution, J. Chem. Soc., Faraday Trans., 93 (1997) 2893-2897.

[18] X. Xiong, B. Sun, J. Zhang, N. Gao, J. Shen, J. Li, X. Guan, Activating persulfate by Fe^0 coupling with weak magnetic field: Performance and mechanism, Water Res., 62 (2014) 53-62.

[19] Y. Zhou, X.L. Wang, C.Y. Zhu, D.D. Dionysiou, G.C. Zhao, G.D. Fang, D.M. Zhou, New insight into the mechanism of peroxymonosulfate activation by sulfur-containing minerals: Role of sulfur conversion in sulfate radical generation, Water Res., 142 (2018) 208-216.

[20] X. Hou, X. Huang, F. Jia, Z. Ai, J. Zhao, L. Zhang, Hydroxylamine promoted goethite surface Fenton degradation of organic pollutants, Environ. Sci. Technol., 51 (2017) 5118-5126.

[21] Y. Feng, H.L. Li, L. Lin, L.J. Kong, X.Y. Li, D.L. Wu, H.Y. Zhao, K. Shih, Degradation of 1,4-dioxane via controlled generation of radicals by pyrite-activated oxidants: Synergistic effects, role of disulfides, and activation sites, Chem. Eng. J., 336 (2018) 416-426.

[22] Y. Feng, D.L. Wu, H.L. Li, J.F. Bai, Y.B. Hu, C.Z. Liao, X.Y. Li, K.M. Shih, Activation of persulfates using siderite as a source of ferrous ions: Sulfate radical production, stoichiometric efficiency, and implications, ACS Sustain. Chem. Eng., 6 (2018) 3624-3631.

[23] A.B. Ross, P. Neta, Rate constants for reactions of inorganic radicals in aqueous solution, US Department of Commerce, National Bureau of Standards Washington D. C, 1979.

[24] D.A. Armstrong, R.E. Huie, S. Lymar, W.H. Koppenol, G. Merényi, P. Neta, D.M. Stanbury, S. Steenken, P. Wardman, Standard electrode potentials involving radicals in aqueous solution: inorganic radicals, BioInorganic Reaction Mechanisms, 9 (2013) 59-61.

[25] P. Neta, R.E. Huie, A.B. Ross, Rate constants for reactions of inorganic radicals in aqueous solution, J. Phys. Chem. Ref. Data, 17 (1988) 1027-1284.
[26] H.H. Kim, H. Lee, H.E. Kim, J. Seo, S.W. Hong, J.Y. Lee, C.H. Lee, Polyphosphate-enhanced production of reactive oxidants by nanoparticulate zero-valent iron and ferrous ion in the presence of oxygen: Yield and nature of oxidants, Water Res. 86 (2015) 66-73.
[27] M. Pirsaheb, S. Moradi, M. Shahlaei, X. Wang, N. Farhadian, A new composite of nano zero-valent iron encapsulated in carbon dots for oxidative removal of bio-refractory antibiotics from water, J. Clean. Prod., 209 (2019) 1523-1532.
[28] C. Kim, J.Y. Ahn, T.Y. Kim, W.S. Shin, I. Hwang, Activation of persulfate by nanosized zero-valent iron (nZVI): Mechanisms and transformation products of nZVI, Environ. Sci. Technol., 52 (2018) 3625-3633.
[29] Y. Wu, X. Chen, Y. Han, D. Yue, X. Cao, Y. Zhao, X. Qian, Highly efficient utilization of nano-Fe (0) embedded in mesoporous carbon for activation of peroxydisulfate, Environ. Sci. Technol., 53 (2019) 9081-9090.
[30] Y.G. Kang, H. Yoon, W. Lee, E.J. Kim, Y.S. Chang, Comparative study of peroxide oxidants activated by nZVI: Removal of 1,4-dioxane and arsenic(III) in contaminated waters, Chem. Eng. J., 334 (2018) 2511-2519.
[31] G. Barzegar, S. Jorfi, V. Zarezade, M. Khatebasreh, F. Mehdipour, F. Ghanbari, 4-Chlorophenol degradation using ultrasound/peroxymonosulfate/nanoscale zero valent iron: Reusability, identification of degradation intermediates and potential application for real wastewater, Chemosphere, 201 (2018) 370-379.
[32] J. Li, X. Zhang, Y. Sun, L. Liang, B. Pan, W. Zhang, X. Guan, Advances in sulfidation of zerovalent iron for water decontamination, Environ. Sci. Technol., 51 (2017) 13533-13544.
[33] Y. Mu, F. Jia, Z. Ai, L. Zhang, Iron oxide shell mediated environmental remediation properties of nano zero-valent iron, Environ. Sci. Nano, 4 (2017) 27-45.
[34] H. Zhang, Y. Ruan, A. Liang, K. Shih, Z. Diao, M. Su, L.a. Hou, D. Chen, H. Lu, L. Kong, Carbothermal reduction for preparing nZVI/BC to extract uranium: Insight into the iron species dependent uranium adsorption behavior, J. Clean. Prod., 239 (2019) 117873.
[35] T. Liu, X. Li, T.D. Waite, Depassivation of aged Fe^0 by divalent cations: correlation between contaminant degradation and surface complexation constants, Environ. Sci. Technol., 48 (2014) 14564-14571.
[36] X.Q. Li, W.X. Zhang, Sequestration of metal cations with zerovalent iron nanoparticles a study with high resolution X-ray photoelectron spectroscopy (HR-XPS), J. Phys. Chem. C, 111 (2007) 6939-6946.

[37] J. Guo, Z. Li, P. Ranasinghe, S. Bonina, S. Hosseini, M.B. Corcoran, C. Smalley, R. Kaliappan, Y. Wu, D. Chen, Occurrence of atrazine and related compounds in sediments of upper Great Lakes, Environ. Sci. Technol., 50 (2016) 7335-7343.
[38] C.M. Wang, D.R. Baer, L.E. Thomas, J.E. Amonette, J. Antony, Y. Qiang, G. Duscher, Void formation during early stages of passivation: Initial oxidation of iron nanoparticles at room temperature, J. Appl. Phys., 98 (2005) 094308.
[39] J. Liu, Z. Sun, Y. Deng, Y. Zou, C. Li, X. Guo, L. Xiong, Y. Gao, F. Li, D. Zhao, Highly water-dispersible biocompatible magnetite particles with low cytotoxicity stabilized by citrate groups, Angew. Chem. Int. Ed., 48 (2009) 5875-5879.
[40] C. Liang, C. Huang, N. Mohanty, R.M. Kurakalva, A rapid spectrophotometric determination of persulfate anion in ISCO, Chemosphere, 73 (2008) 1540-1543.
[41] Z. Ai, Z. Gao, L. Zhang, W. He, J.J. Yin, Core–shell structure dependent reactivity of Fe@Fe_2O_3 nanowires on aerobic degradation of 4-chlorophenol, Environ. Sci. Technol., 47 (2013) 5344-5352.
[42] L. Lu, Z. Ai, J. Li, Z. Zheng, Q. Li, L. Zhang, Synthesis and characterization of Fe−Fe_2O_3 core−shell nanowires and nanonecklaces, Crystal growth & design, 7 (2007) 459-464.
[43] Y. Zhou, J. Jiang, Y. Gao, S.-Y. Pang, J. Ma, J. Duan, Q. Guo, J. Li, Y. Yang, Oxidation of steroid estrogens by peroxymonosulfate (PMS) and effect of bromide and chloride ions: Kinetics, products, and modeling, Water Res., 138 (2018) 56-66.
[44] C. Tan, N. Gao, Y. Deng, J. Deng, S. Zhou, J. Li, X. Xin, Radical induced degradation of acetaminophen with Fe_3O_4 magnetic nanoparticles as heterogeneous activator of peroxymonosulfate, J. Hazard. Mater., 276 (2014) 452-460.
[45] H. Gallard, J. De Laat, Kinetic modelling of Fe (III)/H_2O_2 oxidation reactions in dilute aqueous solution using atrazine as a model organic compound, Water Res., 34 (2000) 3107-3116.
[46] D.L. Ball, J.O. Edwards, The kinetics and mechanism of the decomposition of Caro's acid. I, J. Am. Chem. Soc., 78 (1956) 1125-1129.
[47] Y. Feng, P.H. Lee, D. Wu, K. Shih, Surface-bound sulfate radical-dominated degradation of 1,4-dioxane by alumina-supported palladium (Pd/Al_2O_3) catalyzed peroxymonosulfate, Water Res., 120 (2017) 12-21.
[48] F. Ghanbari, C.A. Martínez-Huitle, Electrochemical advanced oxidation processes coupled with peroxymonosulfate for the treatment of real washing machine effluent: A comparative study, J. Electroanal. Chem., 847 (2019) 113182.

[49] L. Hou, X. Li, Q. Yang, F. Chen, S. Wang, Y. Ma, Y. Wu, X. Zhu, X. Huang, D. Wang, Heterogeneous activation of peroxymonosulfate using Mn-Fe layered double hydroxide: Performance and mechanism for organic pollutant degradation, Sci. Total Environ., 663 (2019) 453-464.

[50] G.V. Buxton, C.L. Greenstock, W.P. Helman, A.B. Ross, Critical review of rate constants for reactions of hydrated electrons, hydrogen atoms and hydroxyl radicals (·OH/·O^-) in aqueous solution, J. Phys. Chem. Ref. Data, 17 (1988) 513-886.

[51] C.L. Clifton, R.E. Huie, Rate constants for hydrogen abstraction reactions of the sulfate radical, SO_4^-. Alcohols, Int. J. Chem. Kinet., 21 (1989) 677-687.

[52] Y. Feng, D. Wu, Y. Zhou, K. Shih, A metal-free method of generating sulfate radicals through direct interaction of hydroxylamine and peroxymonosulfate: Mechanisms, kinetics, and implications, Chem. Eng. J., 330 (2017) 906-913.

[53] Z. Xiong, B. Lai, P. Yang, Y. Zhou, J. Wang, S. Fang, Comparative study on the reactivity of Fe/Cu bimetallic particles and zero valent iron (ZVI) under different conditions of N_2, air or without aeration, J. Hazard. Mater., 297 (2015) 261-268.

[54] C.R. Keenan, D.L. Sedlak, Factors affecting the yield of oxidants from the reaction of nanoparticulatezero-valent iron and oxygen, Environ. Sci. Technol., 42 (2008) 1262-1267.

[55] Y. Pang, Y. Ruan, Y. Feng, Z. Diao, K. Shih, L.a. Hou, D. Chen, L. Kong, Ultrasound assisted zero valent iron corrosion for peroxymonosulfate activation for Rhodamine-B degradation, Chemosphere, 228 (2019) 412-417.

[56] A. Liu, J. Liu, J. Han, W.X. Zhang, Evolution of nanoscale zero-valent iron (nZVI) in water: Microscopic and spectroscopic evidence on the formation of nano- and micro-structured iron oxides, J. Hazard. Mater., 322 (2017) 129-135.